Flow characteristics around an elliptic cylinder placed in the focus of a parabolic solar concentrator of 90°rim angle

M. S. Mostafa, R.M.Kamal and M.H.Gobran
Mechanical Power Dept, Faculty of engineering, Zagazig University, Egypt.

The effect of a parabolic plate on the flow characteristics around an elliptic cylinder placed in the focus of the plate, was experimentally investigated through measurement of the surface pressure distribution, and estimation of flow parameters such as drag and lift coefficients. Also, flow visualization was carried out to clarify the flow patterns around the cylinder. The elliptic cylinder examined has an axis ratio 1:2.17, and a parabolic plate to represent a solar concentrator with rim angle 90° and aspect ratio of 1.5 were used. The angle of attack was changed from 0° to 90° at 15° intervals. The test fluid was air and the Reynolds number based on the major axis length was 3×10^4. It was found that the pressure distribution depends strongly upon the angle of attack, α. On the suction side, Cp (coefficient of pressure) decreases steeply and reaches its minimum. The location of minimum C_P moves upstream with increasing α. On the other hand, the minimum value of C_P on the pressure side moves downstream with an increase of α. For the cylinder/plate combination the form drag increases with α but its values is lower than that of cylinder alone. The location of separation point on the suction side shifts to leading edge at α = 0° and 15° compared with that in the case of cylinder alone. Also as the angle of attack increases the flow on the pressure side separates earlier than that of cylinder alone. For the cylinder-plate combination as α increases form 30° to 75°, the flow on the suction side separates but reattachment occurs. The location of the reattachment point varies clearly with the angle of attack in this range.

يعتبر تطوير المركزات الشمسية ذات القطع المكافئ من المجالات الهامة في بحوث الطاقة المتجددة ، و من هنا تبدو أهمية دراسة طبيعة سريان المائع حول الاسطوانة الموضوعة في بؤرة قطع مكافئ مما يسهم بقدر كبير فى تفسير نتائج انتقال الحرارة حولها. و تتناول الدراسة الحالية إجراء التجارب المعملية لدراسة خصائص سريان المائع حول اسطوانة بيضاوية الشكل موضوعة فى بؤرة قطع مكافئ ذو زاوية حرف ٩٠ درجة و نسبة باعية ١،٥ و نسبة المحورين الأصغر إلى الأكبر ١ : ٢،١٧ مع استخدام الهواء كمائع للدراسة عند رقم X٣ ١٠ ٤ . و قد تمت مقارنة خصائص سريان المائع حول الاسطوانة المنفردة بخصائصه فى حالة و جودها فى بؤرة القطع المكافئ من خلال قياس توزيع الضغط حول سطح الاسطوانة عند زوايا سقوط مختلفة من صفر إلى ٩٠ درجة بمعدل زيادة مقدارها ١٥ درجة حيث أمكن حساب كل من معاملي الجر و الارتفاع و تحديد نقاط انفصال المائع عن سطح الاسطوانة. و قد تم أيضا تصوير شكل السريان حول الاسطوانة عند زوايا السقوط المختلفة مع الاستعانة بالحاسب الشخصي فى تحليل و إظهار الصور المختلفة للسريان. و قد وجد أن قيمة معامل الجر تزداد بزيادة زاوية السقوط ليصل قيمته القصوى عند زاوية ٩٠ درجة فى حين أن معامل الارتفاع يصل لقيمته القصوى عند زاوية سقوط ٤٥ درجة ثم يبدأ في النقصان حتى يصل إلى القيمة صفر عند زاوية ٩٠ درجة ؛ هذا و قد لوحظ بالنسبة إلى انفصال المائع عن سطح الاسطوانة على جانب السحب معاودة الملامسة مرة أخرى عند زوايا سقوط من ٣٠ إلى ٧٥ درجة مع اعتماد موضع الملامسة على زاوية السقوط .

Keywords: Fluid flow, Experimental study, Elliptic cylinders, Parabolic concentrator, Flow visualization.

1. Introduction

Studying the characteristics of fluid flow around an elliptic cylinder placed in the focus of parabolic solar concentrators is important. For some practical applications an elliptic cylinder was placed in the focus of parabolic plate, as in the case of solar concentrators. The wind flow around the absorber tube (elliptic or circular cylinder) in this case is more complicated than that in the free cylinder case. In addition understanding the flow patterns around an interference bodies is useful to explain the heat transfer results around these bodies. According to the relevant literature to the authors, pervious studies directly related to this aspect are almost not existing.

A series of experimental studies upon steady and unsteady flow behaviors of elliptic cylinders have been reported by Modi et al. [1-4]. The mean and fluctuating pressure distributions, the drag, lift, and moment coefficients, the Strouhal number and also the near wake feature were clarified at the subcritical Reynolds number. They described that the aerodynamic characteristics exhibited no dependency upon the Reynolds number in the subcritical flow regime.

Many authors have investigated flow around an elliptic cylinder at moderate and high Reynolds numbers for a long time. The drag coefficients obtained have been cited in references [5, 6]. It can be found that many of such drag coefficients referred by Goldstein [4] decrease steadily with increasing Reynolds number. It was suggested that those data were obtained in the critical flow state. The drag coefficient and the Strouhal number were measured for an elliptic cylinder of axis ratio 1: 2 at two values of angle of attack (α= 0° and 90°) by Delay and Sorensen [7]. All the results at α = 0° extend from the subcritical flow to the supercritical one. The Strouhal number was found to vary discontinuously at the critical Reynolds number. The flow around an elliptic cylinder of axis ratio 1:3 was investigated experimentally in the critical Reynolds number regime by Ota et al. [8]. They found that the critical Reynolds number varies with the angle of attack and attains a minimum around α = 5° to 10°. At the critical Reynolds number, the drag, lift, and moment coefficients change discontinuously, and the Strouhal number reaches a maximum of about 1 to 1.5 depending on the angle of attack.

Numerous studies have also investigated the flow interactions between non-circular bluff bodies. Ball et al. [9], measured the drag force on groups of normal flat plates. The flow interaction between two rectangular cylinders was investigated by Kobayashi [10]. Flow around two elliptic cylinders in tandem arrangement was experimentally investigated by Ota [11]. He measured the surface static pressure distribution around the elliptic cylinders of axis ratio of 1:3. Ota found that the flow characteristics vary drastically with the angle of attack and also the cylinder spacing.

The near wake of smooth circular cylinder had been investigated extensively, for example, Kourta et al. [12], Hayakawa and Hussain [13], and Bays-Muchmore and Ahmed [14]. Based on flow visualization and hot wire measurements, the transition from laminar regime and development of turbulence in the near wake of the cylinder within the subcritical regime of smooth cylinder ($Re_d < 6 \times 10^4$) were studied. Further, Kourta et al. [12] established two Reynolds number flow regimes of $2 \times 10^3 < Re_d \leq 1.6 \times 10^4$ and $1.6 \times 10^4 \leq Re_d < 6 \times 10^4$. In the former regime, laminar wake was identified and transition to turbulence occurred downstream of the cylinder. Within the laminar and transitional wakes there are small scale structures, transition waves or secondary or streamwise vortices, within the two shear layers, in addition to the Karman or Strouhal vortices formed further downstream.

The objective of the present study is to investigate the flow interference between an elliptic cylinder and parabolic plate in subcritical flow regime.

2. Experimental apparatus and technique

Experiments were carried out in two wind tunnels. One of them is used for flow measurements, and the other is used for flow visualization. Measurements were conducted in a low speed wind tunnel discharging air to the atmosphere [15]. The tunnel has a test section of 0.44 x 0.44 m and a length of 1.0 m. During the experiments the flow upstream of the cylinder had uniform velocity profile within ± 1 % of the mean value. The velocity at the entrance of the test section (U_∞) was measured by means of a Pitot tube. The uncertainty in the measured velocity was about ± 0.83 %. The experiments were carried out in the subcritical Reynolds number region ($Re = 3 \times 10^4$).

Flow visualization was carried out in a smoke tunnel that has the working section of 0.18 m width, 0.24 m height, and 0.1m depth, with vertically upward flow. In order to obtain a clear picture of accurate details, the following technique was applied in the present

work. A video camera was used to view and record the smoke visualized flow pattern around the models. The video system was connected to a personal computer through a video card. The output video picture was seen on the computer monitor, and then is captured using spitfire software. This system's unique advantage of variable slow-motion playback, still framing and slow motion reverse playback allowed a detailed and clear picture of the flow pattern. The captured flow pattern pictures were printed later.

2.1. Test model

The test model consists of an elliptic cylinder and parabolic plate with a rim angle of 90°. The elliptic cylinder examined has an axis ratio of 1:2.17, the major axis being 27.6 mm and the span-wise length 440mm. The cylinder was made of wood by the following procedure. Using an elliptic edge cutter tool with major axis of 28 mm and 14 mm minor axis shaped the wooden cylinder. Next, twenty-four longitudinal slots (4-mm depth and 1 mm width) were made on the cylinder's circumference at equal intervals. The slots start from the mid span of the cylinder to the two ends of it. Stainless steel pipes (0.7mm and 0.45mm outside and inside diameters, respectively) were bent from one end at right angle and inserted in these slots. The right angle end of the pipes were inserted perpendicularly on the cylinder surface at the mid span of the cylinder. The other ends of the stainless steel pipes were connected to rubber tubes. Finally the slots were covered with epoxy steel, and the cylinder surface was manually finished. The cylinder was located horizontally at mid height of the test section in the focal plan of the parabolic plate. The surface distance, s, is measured from the leading edge of the cylinder, and it has a positive sign along the suction side and negative sign along the pressure side. The parabolic plate was made of Plexiglas (120mm width and 6 mm thickness) with 1.5 aspect ratio. The profile of the parabola and the focal property can be obtained using the following equations:

$$x = \frac{y^2}{4F}, \tag{1}$$

$$F = \frac{H}{2\sin\varphi}(1+\cos\varphi)\cdot \tag{2}$$

Where x and y are the coordinates of the parabolic plate.

The geometrical characteristics of the parabolic plates are listed in table 1. Fig. 1 shows the cylinder/plate combination.

Table 1
Geometrical characteristics of parabolic plates

W/c	H/c	Φ	W/H	(F/c)
8.295	5.529	90°	1.5	2.765

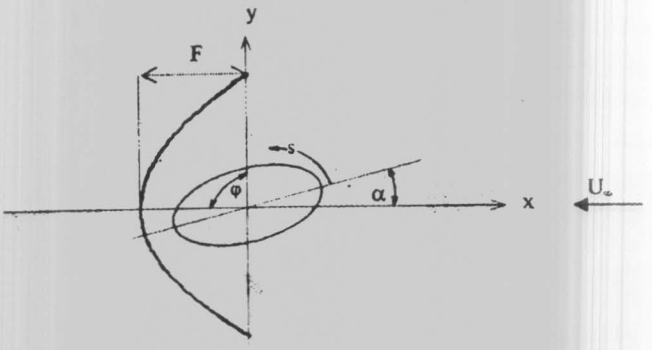

Fig. 1. Cylinder / plate combination.

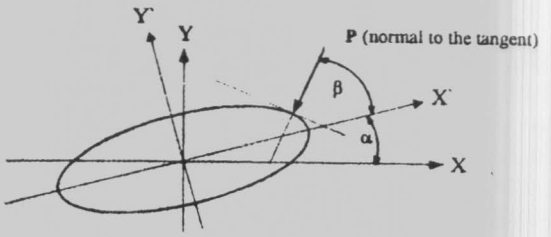

Fig. 2. Pressure vector representation on cylinder surface.

2.2. Flow visualization test model

In the present experiments another elliptic cylinder was used to allow flow visualization. The cylinder was made of Plexiglas of 100 mm length and 15 mm major axis. The plates used for flow visualization were similar to those used in the experimental measurements, and their characteristics are the same for the test model (table 1).

3. Flow parameters

In the present study the flow parameters are pressure coefficient (Cp), form drag coefficient (C_D), and lift coefficient (C_L) .The pressure distribution was measured by Pitot tube together with an electronic micro-manometer. The accuracy of the manometer is ± 0.3 mm H_2O. The Pressure coefficient at any point along the surface is given as $C_P=(P-P_\infty)/(0.5\rho U_\infty^2)$. The uncertainty in pressure coefficient is ± 2.2 %. Assuming incompressible flow condition, the dynamic head $0.5\rho U_\infty^2 = (P_{t\infty}- P_\infty)$, which can be measured. Finally the pressure coefficient is given by,

$$C_P =(P-P_\infty)/(P_{t\infty}- P_\infty). \quad (3)$$

The drag, and lift coefficients (C_D&C_L) based on the major axis of the elliptic cylinder were evaluated from the pressure distribution by the following equations,

$$C_D = \frac{1}{c}\int_s C_p \cos(\beta+\alpha)ds\,, \quad (4)$$

$$C_L = \frac{1}{c}\int_s C_p \sin(\beta+\alpha)ds\,. \quad (5)$$

The above integration were numerically calculated using Simpson-rule. At each point along the cylinder surface (24 points) the angle (β), which is the inclination angle of the pressure vector to the major axis, was determined (for an axis ratio of 1:2.17) from,

$$\beta = \tan^{-1}(4y'/x'). \quad (6)$$

The position of zero angle of attack was carefully determined by comparing the pressure distributions on two sides of the cylinder. Furthermore, comparisons of the present results (drag and lift coefficients) for cylinder alone with previous data were used to check the validity of measurements. It confirmed a reasonable accuracy of the present elliptic cylinder within ± 5 %.

4. Results and discussion

Fig. 3 illustrates the pressure coefficient distribution along the cylinder surface for cylinder/plate combination compared with that of cylinder alone, at different angle of attacks (0° to 90° at 15° interval).

Fig. 3-a represents the pressure distribution for α = 0°. It shows that the pressure distribution versus the surface distance s/c of the cylinder. The static pressure decreases with increasing distance from the stagnation point until it reaches its minimum value at s/c = + 0.31 for cylinder alone, and at s/c = + 0.21 for cylinder/plate combination. Downstream of these positions, the pressure begins to increase. The boundary layer is no longer able to move against the positive pressure gradient, so it separates from the front part of the cylinder at about s/c = 0.86, and -0.86 for cylinder alone and for cylinder/plate combination it separates early at about s/c = 0.64, and -0.64. The separation point determined by a point at which the static pressure begins to be nearly constant.

At α = 15°, the flow is accelerated very rapidly around the leading edge, producing a very steep decrease of Cp as found in fig. 3-b. The flow on the suction and pressure sides separates at s/c = 0.3, and - 0.96, for cylinder alone and at s/c = 0.2, and - 0.6, for cylinder/plate combination respectively.

Figs. 3-c to 3-g show that, for cylinder/plate combination, the static pressure on the suction side after the separation point is constant till a certain location then, it increases again. The flow on the suction side separates and the separated shear layer reattaches onto the cylinder surface. The location of reattachment point depends strongly on the angle of attack in the range from 30° to 75° (see fig. 9). This location approaches to the leading edge as the angle of attack increases.

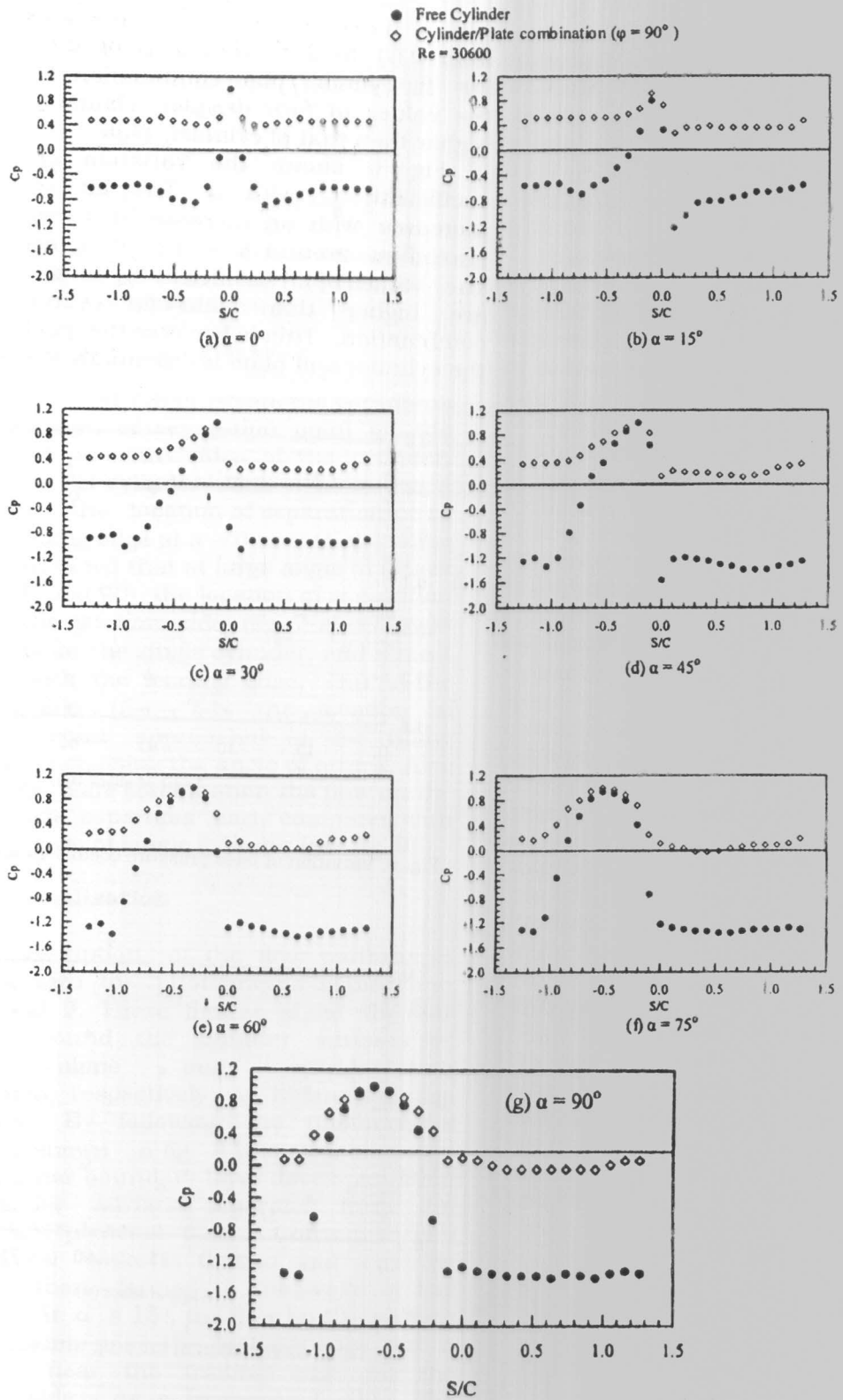

Fig. 3. Pressure distribution around cylinder plate combination.

Needless to say, the pressure distribution varies with the angle of attack. This figure reveals that the upstream stagnation point shifts downstream from the leading edge at α = 0° to the minor axis at α = 90°. For example it locates at about s/c = - 0.11 and -0.64 for α = 15° and 90° respectively. Also it can be seen that, in the case of cylinder / plate combination the values of the static pressure around the cylinder surface are higher than that around the cylinder surface alone. This can be explained as: when the plate is placed normally in a uniform stream a stagnation region is created on its frontal face, therefore, the flow within the gap between the cylinder and plate becomes nearly stagnant, this leads to increase the static pressure on the cylinder surface. For cylinder/plate combination, at all angles of attack the flow on the pressure side separates early compared with the cylinder alone. It can be detected that at large angles of attack such as 45° and 90°, the location of separation point on the suction side is almost the same as for the single cylinder, and almost coincides with the leading edge.

Finally, one can conclude that the pressure distribution depends strongly upon α. On the suction side, Cp decreases steeply and reaches a minimum, whose location moves upstream with increasing α. On the other hand, the minimum value of Cp on the pressure side moves downstream with an increase of α suggesting a downstream shift of the laminar separation point.

The base pressure coefficient Cp_b is defined as a value of Cp at the trailing edge of the cylinder. Referring to fig. 4, it is clear that the base pressure depends on the angle of attack. It decreases with increasing the angle of attack. For cylinder/plate combination the base pressure has a higher value compared with the cylinder alone, because the solid boundary of the plate restricts the wake behind the cylinder and the gap between the cylinder and plate is essentially stagnant.

Fig. 5 shows the variation of drag coefficient, C_D, (based on the major axis, c) with α. It can be seen that C_D increases with α from 0.01 to 0.57 when α changed from 0° to 90° for cylinder/plate combination. For all α's the values of form drag for cylinder alone are higher than that of cylinder/plate

Fig. 6 shows the variation of the lift coefficient, C_L with α. The lift coefficient increases with an increase of α reaching a maximum around α = 45°, then decreases. The values of lift coefficient for single cylinder are higher than that for cylinder/plate combination. This is because the gap between the cylinder and plate is essentially stagnant .

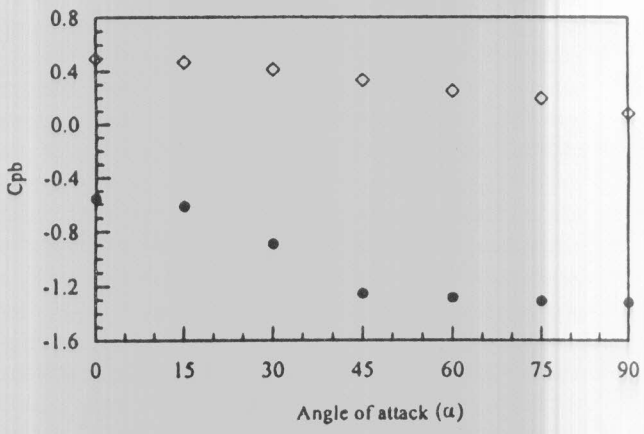

Fig. 4. Variation of base pressure coefficient with α.

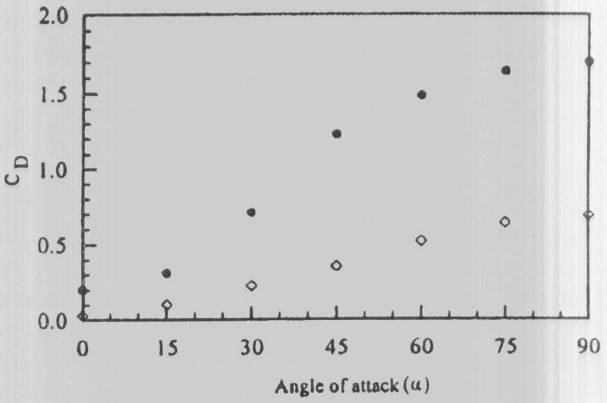

Fig. 5. Variation of for drag with α.

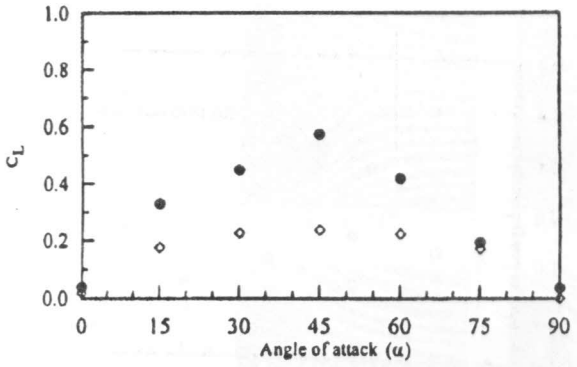

Fig. 6. Variation of lift with α.

Figs. 7-a, and 7-b illustrate the variations of the location of separation point on the suction and pressure sides of the cylinder, respectively. For cylinder/plate combination it is clear that the location of separation point shifts to leading edge at α = 0 and 15 deg. Also it can be detected that at large angle of attack such as 45° and 90°, the location of separation point on the suction side (fig. 7-a) is almost the same as for the single cylinder, and almost coincides with the leading edge. But on the pressure side (fig. 7-b) the location of separation point approaches to the trilling edge with increasing the angle of attack. Also for cylinder/plate combination the flow on the pressure side separates early compared with that in the case of single cylinder (see fig. 9).

5. Flow visualization

The description of the flow patterns is facilitated with the photographs displayed in Figs. 8 and 9. These figures show the flow patterns around the cylinder surface for cylinder alone and cylinder/plate combination, respectively, at different angles of attack. By following the photographs sequence, shown in fig. 8 it is clear that at α = 0°, a laminar boundary layer developing on the cylinder surface separates from the suction and pressure sides. Consequently a very narrow wake is formed and a vortex street is then formed in the wake of the cylinder. At α = 15°, the flow on the suction side separates near the leading edge but it separates near the trailing edge on the pressure side. As α increases further, the position of separation point on the suction side of the cylinder is fixed near the leading edge, although it moves towardes the trailing edge on the pressure side. It is clear that the wake width (the wake width is defined as the distance between the separated shear layers behind the cylinder at one minor diameter from the cylinder center) depends strongly upon α, the wake width increases generally with an increase of α.

Fig. 9 shows the flow pattern around the cylinder-plate combination. When the plate is placed behind the cylinder, the boundary layer separates from the suction and pressure sides of the cylinder. A pair of unsteady opposite singed vortices with rotational directions is formed. These two vortices are impinging the plate surface and closed recirculation region forms between the cylinder and plate. Virtually no exchange of fluid occurs between the air in the gap and the free stream. In this sense, the fluid in the gap can be considered to be recirculating but confined stagnant.

Also it is clear that the position of separation point on the suction side of the cylinder is fixed near the leading edge as α increases form 30 to 90 deg. But on the pressure side it moves towardes the trailing edge with increasing α. As α increases form 30 to 75 deg., the flow on the suction side separates laminarly and the separated shear layer reattaches onto the cylinder surface. The location of reattachment line depends strongly on the angle of attack in this range. Such location approaches to the leading edge as the angle of attack increases.

6. Conclusions

The effect of the present of a parabolic plate on the flow characteristics around an elliptic cylinder was experimentally investigated at Re = 3 x 10^4. It has been found that:

(i) The pressure distribution depends strongly upon the angle of attack (α). On the suction side, coefficient of pressure (Cp) decreases steeply and reaches a minimum, this location moves upstream with increasing α. On the other hand, the minimum value of Cp on the pressure side moves downstream with an increase of α.

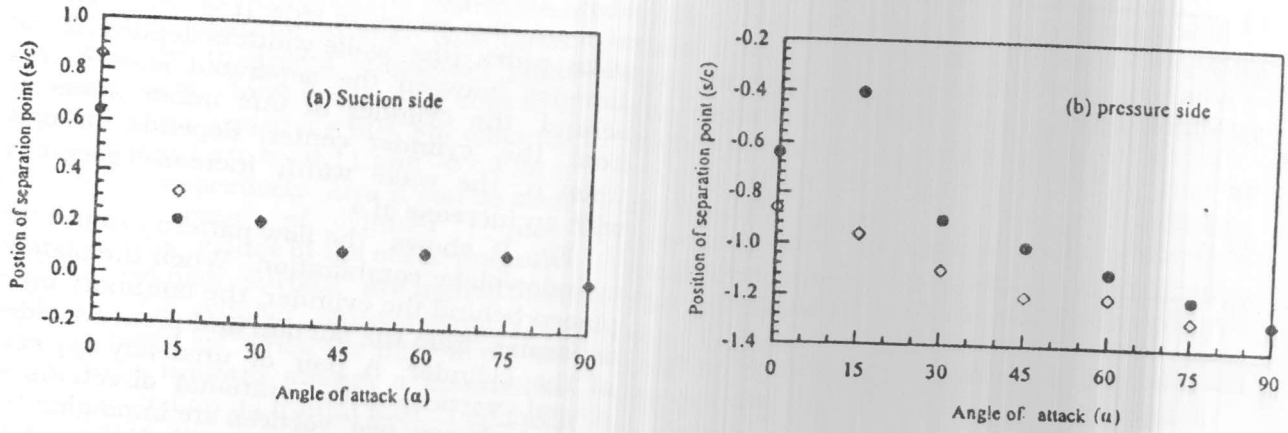

Fig. 7. Variation of separation point position on the cylinder surafce.

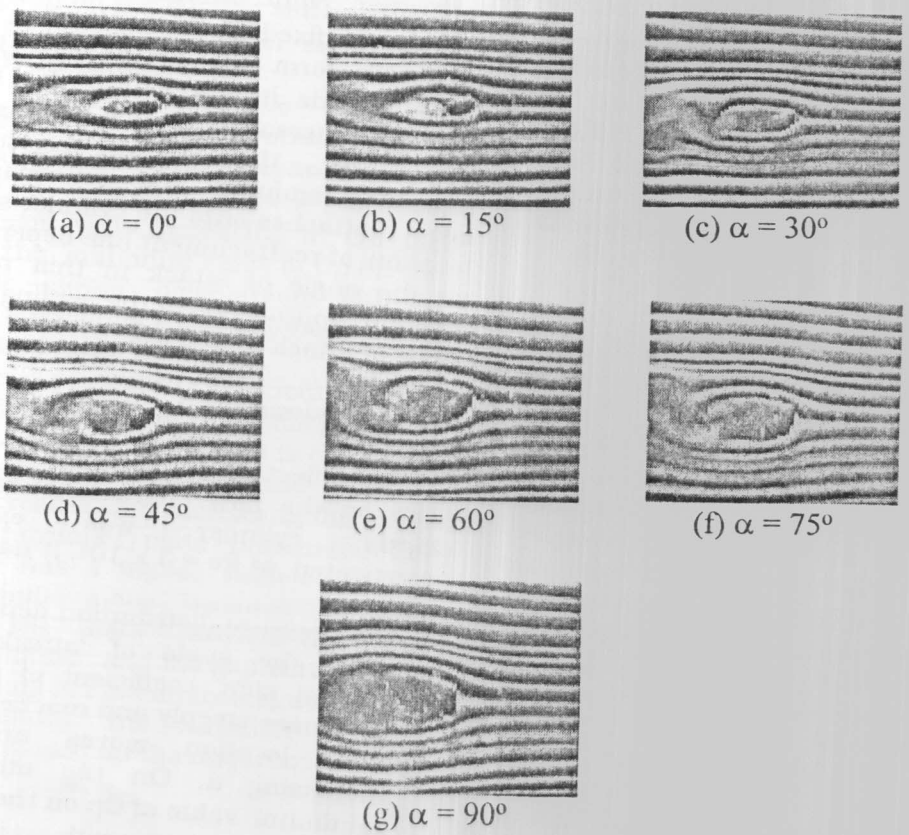

Fig. 8. Flow visualization around an elliptic cylinder.

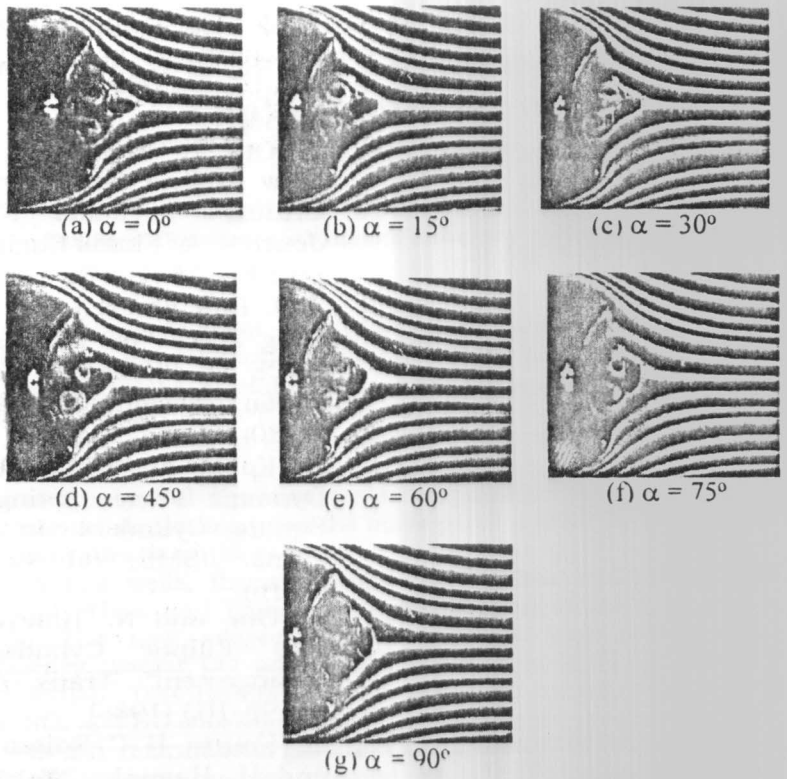

Fig. 9. Flow Visualization around cylinder / plate combination

(ii) For cylinder/plate combination the form drag increases as α increases but its values is lower than that of single cylinder. The location of separation point on the suction side shifts to leading edge at α = 0 and 15° compared with that in the case of single cylinder. Also as the angle of attack increases the flow on the pressure side separates earlier than that of single cylinder.

(iii) The wake width depends strongley upon α, it increases generally with an increase of α.

(iv) The position of separation point on the suction side of the cylinder is fixed near the leading edge as α increases form 30° to 90°. But on the pressure side it moves towardes the trailing edge with increasing α. For cylinder-plate combination as α increases form 30° to 75°, the flow on the suction side separates and the separated shear layer reattaches onto the cylinder surface.

(v) The location of reattachment point depends strongly on the angle of attack in this range. When the plate is placed behind the cylinder, a pair of large unsteady opposite singed vortices or eddies with rotational directions are formed. The fluid in the gap can be considered to be re-circulating in confined region

Acknowledgment

The authors would like to acknowledge Prof. Dr. M. Raafat Shaalan, in mechanical power engineering department, zagazig university for his invaluable contributions to this work.

Nomenclature

C major axis of elliptic cylinder, m

C_D drag coefficient, $D/0.5\ \rho\ U_\infty^2\ c$

C_L lift coefficient, $L/0.5\ \rho\ U_\infty^2\ c$

C_p Pressure coefficient, $P- P_\infty/0.5\ \rho\ U_\infty^2$

C_{pb} base pressure coefficient

D drag, force per unit length (N/m)

F focal length, m

H height of parabolic plate, m
L Lift, force per unit length (N/m)
r position vector
Re Reynolds number = $\rho U_\infty c/\mu$
P_∞ Free stream static pressure, (N/m^2)
$P_{t\infty}$ total free stream pressure, (N/m^2)
U_∞ Free stream velocity, m/s
s surface distance from leading edge, m
W parabolic plate width, m
x, y General coordinates
x', y' Ellipse coordinate
α angle of attack
β pressure-x axis angle
θ coordinate angle
φ rim angle, deg.
μ free stream dynamic viscosity, ($N.s/m^2$)
ρ free stream density, (kg/m^3)

References

[1] V. J. Modi, and E. Wiland, "Unsteady Aerodynamics of Stationally Elliptic Cylinders in Subcritical Flow" AIAA J., Vol. 8, pp. 1814-1821 (1970).

[2] V. J. Modi, and A. K.,Dikshit, "Mean Aerodynamics of Stationally Elliptic Cylinders in Subcritical Flow", Proc. Thrid Int. Conf. On wind effect on buildings and structures, Tokyo, pp. 345-355 (1979).

[3] V. J. Modi, and A. K., Dikshit, "Near-Wakes of Elliptic Cylinders in Subcritical Flow" AIAA J., Vol. 13, pp. 490-497 (1975).

[4] V. J. Modi, and L. Ieong, "On Some Aspects of Unsteady Aerodynamics and Vortex Induced Oscillations of Elliptic Cylinders at Subcritical Reynolds Number", ASME Journal of mechanical design, Vol. 100, pp. 354-362 (1978).

[5] S. Ed. Goldstein, "Moderm Developments in Fluid Dynamic" Vol. II, Oxford Univ. press (1938).

[6] S. F. Hoerner, Fluid-Dynamic Drag, Published by the Author (1985).

[7] N. K. Delay, and N. E. Sorensen, "Low-Speed Drag of Cylinders of Various Shapes" NACA tech. Note, No. 3038, (1953).

[8] T. Ota, H. Nishiyama, and Y. Taoka " Flow Around an Elliptic Cylinder in the Critical Reynolds Number Regime" Journal of Fluids Engineering, Vol. 109, pp 149-155 (1987).

[9] D.J. Ball, and N.J. Cox, "Hydrodynamic Drag Forces on Groups of Flat Plates" ASCE J. Waterway, Port, Coastal and Ocean Division, Vol. 106, pp. 229-238 (1980).

[10] T. Kobayahi, "Characteristics of Fluid Dynamic Forces Acting on Circular or Square Cylinders in Close Proximity" Trans. JSME, Vol. 42, pp. 1452-1461 (1976).

[11] T Ota, and N. Hideya, " Flow Around Two Elliptic Cylinders in Tandem Arrangement" Trans. ASME, Vol. 108, pp. 98-103 (1986).

[12] K. Kourta, H. C. Boisson, P. Chassaing, and H. Haminh, "Nonlinear Interaction and Transition to Turbulence in the Wake of a Circular Cylinder" Journal of Fluid Mechanics, Vol. 181, pp. 141-161 (1987).

[13] M. Hayakawa, and F., Hussain, "Three-Dimensionality of Organized Structures in a Plane Turbulent Wake" Journal of Fluid Mechanics, Vol. 180, pp. 193-229 (1989).

[14] B. Bays-Muchmore, and A. Ahmed, "On Streamwise Vortices in Turbulent Wakes of Cylinders" Physics of Fluids, Vol. A5, pp. 387-392 (1993).

[15] M.S. Mostafa, "Experimental Investigation of Fluid Flow and Heat Transfer Around Circular Cylinder-Flat and Curved Plates Combinations", Ph.D. Thesis, Mechanical Power Engineering, Faculty of Engineering, Cairo University (1998).

Received August 10, 2000
Accepted November 19, 2000